Loss of cardiomyocyte AKT signaling causes deterioration of lipid metabolism and cellular atrophy

Stefanie Gödecke, André Heinen, Tim Appel, Phil-Torben Müller, Tim Stemmer, Daniela Müller, Uli Flögel, Diran Herebian, Fiorella A. Solari, Rene Deenen, Karl Köhrer, Albert Sickmann, Axel Gödecke

Article - Version of Record

Suggested Citation:
Gödecke, S., Heinen, A., Appel, T., Müller, P.-T., Stemmer, T. C., Müller, D., Flögel, U., Herebian, D., Solari, F. A., Deenen, R., Köhrer, K., Sickmann, A., & Gödecke, A. (2026). Loss of cardiomyocyte AKT signaling causes deterioration of lipid metabolism and cellular atrophy. Metabolism, 180, Article 156619. https://doi.org/10.1016/j.metabol.2026.156619

Metabolism 180 (2026) 156619

Contents lists available at ScienceDirect

Metabolism

journal homepage: www.journals.elsevier.com/metabolism

Loss of cardiomyocyte AKT signaling causes deterioration of lipid metabolism and cellular atrophy

Stefanie Gödecke [a], André Heinen [a,g], Tim Appel [a], Phil-Torben Müller [a], Tim Stemmer [a], Daniela Müller [a], Uli Flögel [b], Diran Herebian [c], Fiorella A. Solari [d], Rene Deenen [e], Karl Köhrer [e], Albert Sickmann [d,f], Axel Gödecke [a,g,*]

[a] Department of Cardiovascular Physiology, Medical Faculty and University Hospital Düsseldorf, Heinrich-Heine University Düsseldorf, Germany
[b] Department of Molecular Cardiology, Medical Faculty and University Hospital Düsseldorf, Heinrich-Heine University Düsseldorf, Germany
[c] General Pediatrics, Neonatology, and Pediatric Cardiology, Medical Faculty and University Hospital Düsseldorf, Heinrich-Heine University Düsseldorf, Germany
[d] Leibniz-Institut für Analytische Wissenschaften – ISAS – e.V., Dortmund, Germany
[e] Genomics & Transcriptomics Laboratory, BMFZ, Heinrich-Heine University, Düsseldorf, Germany
[f] Medical Faculty, Medical Proteome Center, Ruhr-University Bochum, Bochum, Germany
[g] Cardiovascular Research Institute Düsseldorf (CARID), Medical Faculty and University Hospital Düsseldorf, Heinrich-Heine University Düsseldorf, Germany

ARTICLE INFO

Keywords:
AKT signaling
Cardiac atrophy
Cardiac lipid metabolism
Perilipins
Heart failure

ABSTRACT

The mammalian heart critically depends on oxidative metabolism of fatty acids, glucose, ketones, and amino acids to meet its extensive ATP demands. AKT/protein kinase B plays a central role in regulating cell growth and metabolism by coordinating an anabolic metabolism in response to insulin or IGF1, particularly by elevating glucose uptake and mTOR activity. Here, we investigated the effect of simultaneous deletion of the two major cardiac isoforms AKT1 and AKT2 on the function and metabolism of the adult mouse heart. Inducible cardiomyocyte specific AKT1 AKT2 double knockout mice developed a rapidly progressing and lethal heart failure with extensive cardiomyocyte atrophy. Metabolic analyses of substrate–specific respiration of mitochondria (respirometry) and of isolated cardiac tissue (Seahorse flux analysis) demonstrated that fatty acid metabolism was severely compromised, whereas glucose metabolism was less affected. Volume-specific in vivo NMR spectroscopy and CrCEST (Creatine chemical exchange saturation transfer) imaging revealed a drop of the cardiac phosphocreatine/ATP ratios from 2 to 1.5, indicating severe energetic depletion. Transcriptomic and proteomic studies showed that genes of the TCA cycle, β-oxidation, and oxidative phosphorylation were coordinately downregulated. Moreover, AKT1/AKT2 deficient cardiomyocytes lost the ability to store fatty acids in lipid droplets (LDs) due to an early loss of perilipins and other proteins involved in LD generation and function. In conclusion,

Abbreviations: ADP, adenosine diphosphate; ANOVA, analysis of variance; AP_{max}, arterial systolic pressure; AP_{mean}, mean arterial pressures; AP_{min}, arterial diastolic pressure; BPTES, glutaminase inhibitor; BSA, bovine serum albumin; CCCP, carbonyl cyanide chlorophenylhydrazone; CMA, chaperone-mediated autophagy; CrCEST, creatine chemical exchange saturation transfer; Ctrl, control; Cx43, connexin43; DEG, differentially expressed gene; dP/dt_{max}, maximum rate of pressure change; dP/dt_{min}, minimum rate of pressure change; FA, fatty acid; FAC, fractional area change; FA-CoA, fatty acyl-CoA; FCCP, carbonyl cyanide p-trifluoromethoxyphenyl hydrazine; FIA-MS/MS, flow injection analysis-tandem mass spectrometry; FITC, fluorescein isothiocyanate; FS, fractional shortening; i.p., intraperitoneal; iCM-AKT1, inducible cardiomyocyte specific AKT1 knockout; iCM-AKT12, inducible cardiomyocyte specific AKT1 AKT2 double knockout; iCM-AKT2, inducible cardiomyocyte specific AKT2 knockout; IGF1, insulin-like growth factor 1; IPA, Ingenuity Pathway Analysis; KO, knockout; LCFA, long chain fatty acid; LC-MS/MS, liquid chromatography-tandem mass spectrometry; LD, lipid droplet; LVAW, left ventricular anterior wall; LVEDV, left ventricular end-diastolic volume; LVESV, left ventricular end-systolic volume; LVID, left ventricular inner diameter; LVPED, LV end-diastolic pressure; LVP_{max}, maximal left ventricular pressure; LVPW, left ventricular posterior wall; mCm, merCremer; MS/MS, tandem mass spectrometry measurement; mTOR, mammalian target of rapamycin; MUFA, monounsaturated fatty acid; NGS, normal goat serum; NEFA, non-esterified fatty acid; NPPA, atrial natriuretic peptide; NPPB, brain natriuretic peptide; OCR, oxygen consumption rate; OH-Txf, 4-hydroxytamoxifen; P/O ratio, phosphate/oxygen ratio; PBS, phosphate-buffered saline; PCaa, diacyl-phosphatidylcholine; PCae, acyl-alkyl-phosphatidylcholine; PCr, phosphocreatine; PKC, protein kinase C; PLIN, perilipin; PUFA, poly-unsaturated fatty acid; RM, repeated measure; RPS6, ribosomal protein S6; SFA, saturated fatty acid; TAG, triacyl-glycerol; TCA cycle, tricarboxylic acid cycle; UK5099, mitochondrial pyruvate carrier inhibitor; UPLC-MS/MS, ultra-performance liquid chromatography-tandem mass spectrometry; WGA, wheat germ agglutinin.

* Corresponding author at: Department of Cardiovascular Physiology, Medical Faculty and University Hospital Düsseldorf, Heinrich-Heine University, Postfach 101007, 40001, Düsseldorf, Germany.
E-mail address: axel.goedecke@hhu.de (A. Gödecke).

https://doi.org/10.1016/j.metabol.2026.156619
Received 4 November 2025; Accepted 8 April 2026
Available online 11 April 2026

our data show that general, isoform-independent AKT signaling in cardiac myocytes is indispensable for preservation of cardiac fatty acid metabolism and energy supply.

1. Introduction

The mammalian heart critically depends on sustained substrate and oxygen supply, because large amounts of energy are required to ascertain continuous pump function and ion transport processes. The extensive ATP demand can only be met by oxidative phosphorylation, making the heart an obligatory aerobic organ. A high mitochondrial density of 30–35% of cardiomyocyte volume underlines the dependence on oxidative ATP supply [1]. To assure the pump function even under conditions of varying substrate availability, the heart has a high metabolic flexibility and can switch between fatty acids, glucose, and ketone bodies for ATP generation, but it usually prefers fatty acids as substrate [2]. Since the heart stores only small amounts of substrates in the form of lipids or glycogen, substrate uptake and oxidation must be coordinated to avoid shortage as well as superfluous substrate uptake, as the latter can lead to extensive accumulation of metabolic intermediates in cardiomyocytes. For example, fatty acids that are not utilized for oxidation can accumulate in the cytosol and may be further metabolized to sphingosines and ceramides. These potentially lipotoxic metabolites can act as signaling molecules and may induce cardiac dysfunction and insulin resistance [3]. As with other organs, such as the liver, the heart has the capacity to store excess lipids in the form of lipid droplets (LD). However, the cardiac lipid storage compartment is relatively small and highly dynamic. An adequate supply with substrate and oxygen, intact mitochondria, and proper handling of excess fatty acids are essential requirements to ensure long-term cardiomyocyte function.

AKT/Protein kinase B is an important regulator of cellular growth and metabolism. Extracellular signals such as insulin or IGF1 activate AKT signaling via the PI3-kinase pathway. In general, AKT activation coordinates an anabolic metabolism, with increased glucose and enhanced energy storage in form of glycogen. In addition, AKT contributes to the regulation of cell size and proliferation by controlling protein biosynthesis and autophagy via mTOR signaling.

AKT functions are executed by three AKT isoforms (AKT1–3), which display a high degree of structural homology. Despite their similarity, phosphoproteomic analysis of cardiac myocyte cell lines demonstrated that AKT1 and AKT2, the major isoforms expressed in the heart [4,5], are able to phosphorylate proteins in an isoform-specific manner, but also modify common targets [6]. Isoform-specific AKT knockout mice were important for uncovering AKT functions. Constitutive, global AKT1 deletion in mice particularly affected cell growth, cell survival [7], and physiological cardiomyocyte hypertrophy [8]. In contrast, global AKT2 deletion caused metabolic defects such as disturbed glucose homeostasis with decreased glucose tolerance, insulin resistance [9], and decreased glucose uptake into cardiomyocytes [10]. AKT1 or AKT2 single knockout mice were viable and fertile, whereas constitutive AKT1/AKT2 double knockout mice died shortly after birth [11], and the combined inducible global deletion of AKT1 and AKT2 in adult mice caused rapid weight loss and death [12]. These findings suggest that the overlapping functions executed by both, AKT1 or AKT2, are indispensable for postnatal growth and homeostasis of the adult organism.

In view of the importance of AKT for cardiomyocyte homeostasis, it came as a surprise that the combined cardiac inactivation of AKT1 and AKT2 achieved by conditional deletion of AKT2 in cardiomyocytes of adult, global AKT1 KO mice resulted only in a moderate cardiac phenotype. Hearts of these mice showed reduced contractility as well as lower expression of gap junction and mitochondrial proteins [13], whereas general cardiac structure and survival were not affected. To elucidate the functional and metabolic consequences of the simultaneous loss of AKT signaling in cardiac myocytes for the adult heart and, in particular, the impact on cardiac metabolism, we generated and analyzed inducible cardiomyocyte-specific AKT1/AKT2 double knockout mice (iCM-AKT12). We provide evidence that AKT signaling is indispensable to maintain structure and function of the adult murine heart. The simultaneous loss of both isoforms leads to a rapidly proceeding, complex heart failure. Early after AKT1 and AKT2 inactivation, cardiomyocytes lose the ability to normally store and metabolize fatty acids, followed by extensive disturbance of substrate and energy metabolism, pronounced changes in the cardiac transcriptome, energetic depletion, cardiac cellular atrophy, and eventually premature death.

2. Materials and methods

2.1. Animal procedures

Animal experiments were performed according to the guidelines from Directive 2010/63/EU of the European Parliament and the local animal care and use committee (LANUV Recklinghausen, Germany, License no AZ: 84–02.04.2014.A308, AZ: 81–02.04.2019.A244). Mice were housed in groups of 2 per cage at constant room temperature on a 12-h light/dark cycle with ad libitum access to water and food. Tamoxifen-inducible cardiomyocyte-specific AKT1 or AKT2 single (iCM-AKT1, iCM-AKT2) or AKT1/AKT2 double knockout mice (iCM-AKT12) were generated as described in Supplemental Methods S1.1. Knockout induction and control mice used in this study are described there as well. Functional measurements and organ harvesting were performed at comparable times of the day. After transport, animals were kept in a climate-controlled cabinet (22 °C, humidity 50%) for at least two hours to minimize stress.

2.2. Insulin stimulation

After a fasting period of 4 h, mice were i.p. injected either with saline (= basal) or with insulin (3 U/kg body weight = stimulated) 15 min prior to organ harvesting.

2.3. Measurement of cardiovascular function in anesthetized mice

For repetitive echocardiography, a Vevo 2100 High Frequency Ultrasound System (Visualsonics, Toronto, Canada) with a MS400 transducer (18–38 MHz) was used as described previously [14]. Details of the measurements are described in Supplemental Methods S1.2. Left ventricular and aortic pressure measurements were performed as described [15].

2.4. Cardiac magnetic resonance imaging and spectroscopy

Repetitive in vivo cardiac magnetic resonance imaging of anesthetized mice was performed essentially as described [16]. Details of measurements are described in Supplemental Methods S1.3.

2.5. Isolation of adult cardiomyocytes

Adult cardiomyocytes were isolated from freshly harvested hearts as described and seeded on laminin- coated coverslips for overnight culture [17]. For cell size determinations, unstained cells were analyzed by phase contrast microscopy, and cell length, cell width, and cell areas were measured using the Fiji image-processing package [18]. For induction of LD formation, cells were cultivated for 16 h in the presence of 50 μM BSA alone or 100 μM of oleic acid complexed to BSA in a molar ratio of 2 (oleic acid) to 1 (BSA) (Sigma O3008). For staining, cells were washed with PBS, fixed with 4% formaldehyde for 15 min, washed again

twice with PBS, and blocked in PBS 0.2% saponin 10% normal goat serum (NGS). Cells were then either stained with 0.2% oil red solution in 60% isopropanol for 10 min, followed by 4 washing steps with H_2O, or incubated with primary antibodies (Supplemental Table 1) in PBS 0.2% saponin 2% NGS over night at 4 °C. On the next day, cells were washed with PBS and were incubated with secondary antibody in PBS 0.2% saponin 2% NGS for 1 h. After washing, cover slips were mounted on glass slides with ProLong™ Diamond Antifade Mountant (Thermo Fisher Scientific).

2.6. Isolation of cardiac tissue

Mice were sacrificed by cervical dislocation. After heart dissection, atria were removed and ventricular weight was determined. For RNA and protein analyses, left ventricular heart tissue was frozen in liquid nitrogen. For histological studies, hearts were OCT-embedded and snap frozen in −40 °C cold isopentane.

2.7. Histological analyses

4 μm frozen heart tissue sections were stained with the antibodies listed in Supplemental Table 1 or with FITC-wheat germ agglutinin (WGA) as described [19,20]. For detection of apoptotic cells in cardiac tissue sections, Click-iT™ Plus TUNEL Assay for in situ Apoptosis Detection, Alexa Fluor™ 488 dye, ThermoFisher Scientific (C10617) was used according to the manufacturer's instructions. Fluorescence and phase contrast microscopy was performed with a Keyence BZ 9000 microscope. Confocal fluorescence microscopy was performed with a Zeiss LSM 780 microscope. For analyses of microscopical pictures, Fiji image-processing package was used [18]. LD density in isolated, oleic acid exposed cardiomyocytes was determined by counting the number of perilipin3-positive vesicles in confocal images of single cells. Double staining showed that all PLIN3-positive vesicles were also PLIN2 or PLIN5 positive. A minimum of three cardiomyocytes were analyzed per individual mouse and genotype.

2.8. Western blot analyses

Protein extracts were isolated from left-ventricular tissue and used for Western blotting as described [19]. Antibodies are listed in Supplemental Table 2.

2.9. Protease measurements

Chymotrypsin-like and caspase-like activity of the 26S-proteasome and calpain activity were measured in heart extracts as described [21] using Proteasome-Glo™ Assay (Promega) and Calpain-Glo™ Protease Assay (Promega). 5 μg of cardiac protein was used for each measurement. Luminescence rates at room temperature were registered after 20 min of incubation, when a stable plateau phase was reached, and normalized to protein input.

2.10. Proteomic analysis of mouse heart tissue

Left-ventricular heart tissues of control ($Ctrl^{Cre+}$) and iCM-AKT12 knockout mice isolated and snap-frozen on d21 were used for proteomic analysis as described in detail in Supplemental Methods S1.4.

2.11. Mitochondrial oxygen consumption

Cardiac mitochondria were isolated by differential centrifugation, and ADP stimulated respiration (state 3) and resting respiration (state 4) were measured using complex I substrate (pyruvate/glutamate/malate) or complex II substrate (succinate in combination with complex I inhibitor rotenone) as described [22]. Palmitoyl-L-carnitine was used in a final concentration of 40 μM.

2.12. Measurement of tissue oxygen consumption rates

Cardiac substrate metabolism in intact cardiac tissue slices was determined by extracellular flux analysis using a Seahorse XFe24 extracellular flux analyser as described [23]. Tissue pieces of standardized volume (0.425 mm^3) from iCM-AKT12 knockout or control animals ($Ctrl^{fl/fl}$) at day 21 after the start of OH-Txf treatment (d21) were used. Substrate metabolism was investigated by offering either glucose/pyruvate/glutamine or palmitate/glucose/glutamine as substrate combinations. Oxygen consumption rates (OCR) were measured at baseline and after mitochondrial uncoupling with FCCP (uncoupled), and coupling ratios were calculated as uncoupled/basal OCR. No additional normalization of OCR values was performed, as the same tissue volumes were measured in all wells (volume normalization). In order to determine the dependencies on a specific substrate, long chain fatty acid (LCFA) metabolism was inhibited by etomoxir, glucose oxidation by UK5099, or glutamine metabolism by BPTES in parallel experiments. After administration of one inhibitor, the two other inhibitors were applied together to determine the overall contribution of the three exogenously applied substrates (all pathway inhibition). Substrate dependencies are presented as relative values to all pathway inhibition.

2.13. Metabolomic characterization

Snap-frozen left-ventricular heart tissues of control ($Ctrl^{Cre+}$) and iCM-AKT12 knockout mice were used for metabolomic and lipidomic analyses as described in detail in Supplemental Methods S1.5. Measurements of blood glucose, blood β-hydroxybutyrate, and plasma non-esterified fatty acids (NEFA) concentrations were performed as described in Supplemental Methods S1.6.

2.14. Gene expression analyses

RNA was isolated from left ventricular heart tissue using Fibrous Tissue RNeasy Kit, Qiagen (#74704) according to manufacturer's instruction as described [19].

2.14.1. Microarray analyses

Microarray analyses were performed using *Agilent SurePrint G3 Mouse GE 8 × 60 K Microarrays* as described [19]. Microarray data were analyzed using the *IPA Ingenuity Pathway Analysis software Package* (Qiagen Inc. 2016). Canonical pathways and upstream regulators tools were used to identify affected regulatory networks. Microarray data are accessible via GEO accession number GSE86230 (day 10) and GSE86231 (day 21).

2.14.2. Quantitative real time-PCR (qPCR)

Expression levels of specific genes were determined as described [19] and normalized to the expression of a reference gene identified with unaltered expressions in d10 and d21 array analyses (*Trmt10c* for genes with low expression levels, *Kdelr1* for genes with higher expression levels), and then compared with control groups using the X(0) method [24]. For primer sequences see Supplemental Table 3.

2.15. Statistical analysis

Data analyses were performed in blinded fashion. Data of multiple measurements are presented as mean ± standard deviation (SD). Statistical analyses were performed with Graph Pad Prism 10 as indicated in Figure Legends. For comparison of two groups, two-tailed *t*-tests were used. For comparison of more than two groups, one-way ANOVA followed by multiple comparison tests as indicated in Figure Legends were used. Measurements with two variables (time and genotype) were analyzed by two-way ANOVA followed by multiple comparison tests as specified. Differences were considered as significant at $p < 0.05$.

3. Results

3.1. Cardiac AKT deletion blunts insulin-dependent PI3K/AKT- signaling

Inducible cardiomyocyte-specific single (iCM-AKT1 and iCM-AKT2) as well as double knockout mice (iCM-AKT12) were generated as described in Supplemental Methods S1.1 and Fig. S1. Gene deletion efficiently reduced cardiac AKT expression to 15% for AKT1 and 12% for AKT2 with no compensatory up-regulation of the non-deleted AKT isoforms (Fig. S2A–D), and the vast majority of cardiomyocytes was free of AKT in immunohistological stainings (Fig. S2E).

Next, we investigated the effect of gene deletion on insulin-stimulated, AKT dependent phosphorylations. As shown in Fig. S3A and B, insulin did not stimulate the phosphorylation of the direct AKT target PRAS40 (T246), the indirect AKT targets p70S6 kinase (T389), and RPS6 (S235/336) over basal levels in iCM-AKT12 hearts, whereas stimulated iCM-AKT1 and iCM-AKT2 hearts displayed reduced phosphorylation level as compared to stimulated control hearts. In case of the translational repressor 4E-BP1, which is phosphorylated by mTORC1 in an insulin/AKT dependent manner [25], the hyper-phosphorylated (repressor-inactive) γ-form was dominant in stimulated control, iCM-AKT1-, and iCM-AKT2 hearts, whereas in basal control hearts as well as in stimulated iCM-AKT12 hearts, the hypo-phosphorylated β- and α-forms (repressor-active) were more prominent (Fig. S3C). We therefore conclude that both cardiac AKT isoforms contribute to the insulin-dependent phosphorylation of the investigated target proteins in an additive manner. The loss of both isoforms in iCM-AKT12 resulted in basal phosphorylation, which could not be increased by insulin.

3.2. AKT deletion reduces heart function

After induction of gene deletion, KO mice showed normal general condition and behavior (motility, food intake, breathing), resulting in similar body weights as compared to control mice of the same age (Fig. S2F). However, starting on day 21 only iCM-AKT12 mice showed reduced motility, increasing weakness, and reduced food intake, while the single KO mice showed no impairments. Eventually, iCM-AKT12 mice died between day 21 and day 28 (Fig. 1A). To investigate whether the iCM-AKT12 mice died from impaired heart function because of AKT deletion, we followed cardiac function by weekly serial transthoracic echocardiography starting on d0 (i.e. before start of OH-Txf injection). As shown by quantitative echo data (Fig. 1B), in representative M-mode recordings (Fig. 1C), and in Supplemental Movies 1–4, iCM-AKT12 hearts developed a progressive increase of left ventricular end-systolic volume (LVESV) with constant left ventricular end-diastolic volume (LVEDV), resulting in a decrease of stroke volume, ejection fraction, and cardiac output. In addition, fractional shortening (FS) and fractional area change (FAC) decreased with time, whereas heart rate remained unchanged. In contrast, iCM-AKT1 and iCM-AKT2 single KO mice showed no alterations in cardiac function over the

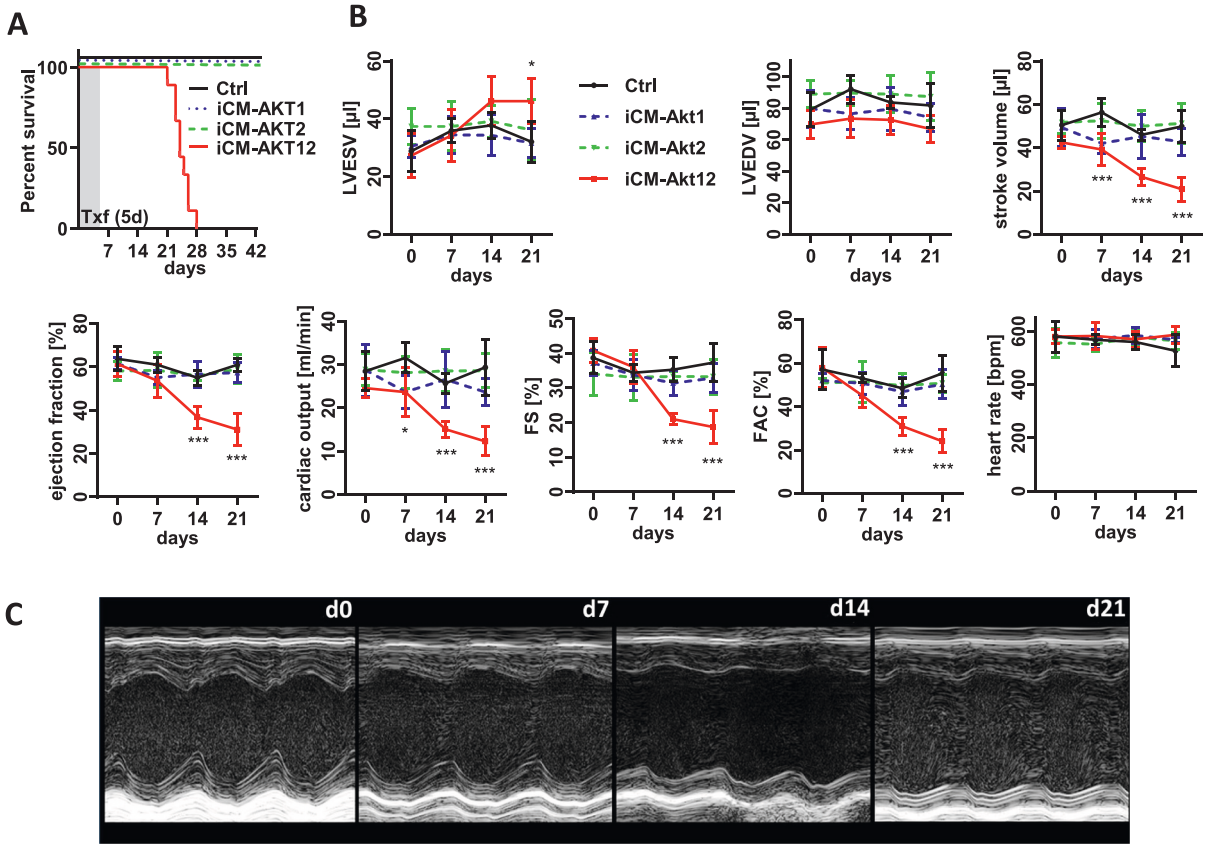

Fig. 1. Combined deletion of AKT1 and AKT2 (iCM-AKT12) but not single deletion of AKT1 (iCM-AKT1) or AKT2 (iCM-AKT2) induces loss of cardiac function.
A: Kaplan-Meier survival curves show the survival probability (%) of Ctrl ($Ctrl^{Cre+}$) and KO mice (n = 9 per genotype).
B: Echocardiographic measurements of heart function of Ctrl ($Ctrl^{Cre+}$) and AKT knockout mice (n = 5 per genotype) at baseline and 7, 14, and 21 days after first OH-Txf injection. LVESV = left ventricular end systolic volume, LVEDV = left ventricular end diastolic volume, FS = fractional shortening, FAC = fractional area change. Heart rates are given in beats per minute (bpm). Ctrl: black line, iCM-AKT1: blue dotted line, iCM-AKT2: green dotted line, iCM-AKT12: red line. Statistical analysis was performed using two-way ANOVA (RM) followed by Šidák's multiple comparison test to compare all knockout groups to control at each time point. * $p < 0.01$, ** $p < 0.01$, ***$p < 0.001$.
C: M-Mode images of short axis of iCM-AKT12 hearts at baseline (d0) and 7, 14, and 21 days after first OH-Txf injection. (For interpretation of the references to colour in this figure legend, the reader is referred to the web version of this article.)

observation period of 21 days. These data suggest that the combined AKT1/AKT2 deletion depressed contractile force. In fact, invasive pressure measurements in the left carotid artery and left ventricle showed that arterial systolic (AP_{max}), diastolic (AP_{min}), and mean pressures (AP_{mean}) as well as maximal left ventricular pressure (LVP_{max}), dP/dt_{max}, and $-dP/dt_{min}$ were compromised in iCM-AKT12 mice, whereas LV end-diastolic pressure (LVP_{ED}) was not altered (Fig. S4).

3.3. AKT deletion induces cardiac cellular atrophy

Microscopical analysis of FITC-WGA stained cardiac sections showed a substantial thinning of the left ventricular wall of iCM-AKT12 hearts that apparently developed between d10 and d21. Stronger FITC-WGA staining suggested an increase of matrix deposition in iCM-AKT12 hearts on d21 (Fig. 2A). Determination of ventricular weight/body weight ratios revealed that ventricular mass was mainly lost between d7 and d14 (Fig. 2B), while body weights remained stable in iCM-AKT12 mice (Fig. S2F). In female mice, ventricular weight/body weight was equally reduced on d21 (Fig. S2G). Analysis of cell sizes in preparations of control and iCM-AKT12 cardiomyocytes isolated on d7, d14, and d21 revealed a progressive cellular atrophy (Fig. 2C,D). On d14 and d21, cell surface area and cell width were reduced by 15% and 20%, whereas cell length was only mildly affected (−7%) (Fig. 2D). Since the function of AKT as a repressor of autophagy is well described [26,27], it was not surprising that we found evidence for increased autophagy in iCM-AKT12 hearts. Increased nuclear localization of the autophagy regulating transcription factor FoxO3A in cardiomyocytes was evident on d21 (Fig. S5A,B). Transcription of autophagy-related genes such as *Bnip3, Gabarapl1, Sqstm1*, or *Ctsl,* was increased from d10 (Fig. S5C). Finally, we observed an increase in free amino acids in heart tissue on d14 (Supplemental Table 4). Apoptosis or proteolytic degradation appeared to play a subordinate role in the development of cardiac atrophy, as they were only moderately increased in end-stage heart failure on d21 (Fig. S5D–F).

3.4. Deletion of AKT leads to global changes in cardiac gene expression

Unbiased transcriptomic analyses of control and iCM-AKT12 heart tissue detected 3783 differentially expressed genes (DEG) in d21 iCM-AKT12 hearts ($p < 0.01$) (Suppl. Table 5; Fig. 3A). Ingenuity pathway analysis (IPA®, Qiagen) showed that pathways related to mitochondrial function (e.g. TCA cycle/respiratory electron transport, oxidative phosphorylation, FA β-oxidation, sirtuin signaling pathway) were globally down-regulated (Fig. 3B). Consistently, the transcription factors PGC-1α (Ppargc1a) (*Z*-score −7.6) and PPARA (Z-score −3.9) were among the upstream regulators and thus might have contributed to the observed alterations of mitochondrial gene expression (Fig. 3C). The expression of the master regulator of mitochondrial biogenesis, PGC-1α, was not altered neither on RNA nor protein level (Fig. S6A). However, transcription of other regulators of mitochondrial gene expression were down-regulated on d21, including the PGC-1α binding partners PPARA and RXRa [28] (Supplemental Table 6). In addition, the day 21 data pointed towards elevated protein synthesis, because related terms appeared among the most upregulated pathways (translation elongation, EIF2 signaling, rRNA processing). This finding was most likely due to the concerted upregulation of ribosomal protein genes included in these pathways in iCM-AKT12 hearts (Fig. S7A,B,C). c-MYC, a main stimulator of ribosomal biogenesis [29], was also found among the upstream activators (*Z*- score 3.1), and c-MYC expression was markedly upregulated in iCM-AKT12 hearts (Fig. S7D). p53 was also inferred to be upregulated (Z-score 6.6). Upregulation of c-MYC and p53 is well known for various pathological conditions in the heart [30,31].

A similar analysis on day 10 showed only very moderate changes in the transcriptome (565 DEG, $p < 0.05$) Nevertheless, it is noticeable that the carnitine metabolism pathway was already down-regulated (Fig. 3D). Moreover, upregulation of cellular stress and protein degradation pathways was found (FOXO-mediated transcription, UPR, ER stress, mitophagy). Upstream regulator analysis highlighted only few candidates, all with relatively low activation *Z*-scores. Remarkably, PGC-1α (Ppargc1a) was the transcriptional regulator with the most negative Z-score (−2.2), while Foxo1 was the transcriptional regulator with the most positive Z-score (3.4) (Fig. 3E). On the level of individual genes, the cardiac stress markers *NPPA* and *NPPB* (encoding atrial natriuretic peptide and brain natriuretic peptide) were already increased on d10, as confirmed by quantitative RT-PCR (Fig. S6B). Remarkably, expression of the *Gja1* gene encoding connexin 43 that was reported to be significantly reduced in hearts of global AKT1 KO mice with conditionally inactivated AKT2 gene [13] was not altered in iCM-AKT12 hearts (Fig. S6C). Although changes at RNA level not necessarily cause changes at protein level, these data suggest that a compromised fatty acid metabolism, mitochondrial dysfunction, and elevated autophagy might be early contributors to heart failure.

Proteomic analysis of d21 control and iCM-AKT12 heart tissue revealed extensive alterations in protein abundancies. Among the 3484 proteins quantified in all analyzed samples (minimum 2 peptides), 486 proteins were differentially regulated. Remarkably, among the 201 significantly downregulated proteins, 123 belong to the mitochondrial proteome (Supplemental Table 7). Comparison of proteomic and transcriptomic data (d21) using the IPA upstream regulator tool resulted in the identification of similar upstream regulators altered in the same directions (Fig. S8A). Moreover, for more than 50% of the regulated proteins we found corresponding significant alterations in the d21 transcriptome, underlining that the transcriptional changes widely translated into altered protein abundancies. On the level of individual proteins, cardiac stress markers NPPA, MYH7, and NPPB were the most upregulated proteins quantified, whereas - besides AKT1 and AKT2 -the lipid droplet associated proteins perilipin2 (PLIN2) and perilipin5 (PLIN5) were the most downregulated proteins quantified (Fig. S8B). Furthermore, proteins involved in various steps of fatty acid (FA) oxidation, like for example in FA-CoA formation (ACSL1), FA import into mitochondria via the carnitine shuttle (CPT1b, SLC25A20/CACT, CPT2), and mitochondrial β-oxidation (ECH1, HADH, ACAA2) were strongly down-regulated (Fig. S8C).

3.5. AKT deficiency impairs metabolic capacity of cardiac tissue

We next asked whether altered mitochondrial protein expression led to functional impairment and performed respirometric measurements on cardiac mitochondria isolated from d21 control and KO hearts (Fig. 4A). Mitochondria were supplied with either complex I substrate (pyruvate/glutamate/malate), complex II substrate (succinate + rotenone), or palmitoyl-L-carnitine. Uncoupled mitochondrial O_2-consumption (CCCP) was only slightly lower in iCM-AKT12 mitochondria as compared to control when either complex I or complex II substrates were offered. The most significant reduction in OCR was observed when palmitoyl-L-carnitine was used (Fig. 4B). Supplemental Table 8 shows a comparable, substrate-specific reduction in ADP-stimulated respiration, where O_2-consumption rates (State 3) of control and iCM-AKT12 mitochondria were comparable when complex I or complex II substrates were offered, but were significantly lower in iCM-AKT12 mitochondria when palmitoyl-L-carnitine was used. Furthermore, the P/O ratio, which is a marker of the efficiency of oxidative phosphorylation, was reduced in iCM-AKT12 mitochondria for all substrates. In summary, AKT deletion resulted in substrate independent deteriorations of mitochondrial bioenergetics as well as in substrate specific impairments that were related to FA metabolism.

Next, Seahorse extracellular flux analyses on tissue slices from control and iCM-AKT12 hearts on d21 were performed to investigate whether the measured mitochondrial dysfunction also led to metabolic impairments in intact tissue (Fig. 4C). Slices of iCM-AKT12 cardiac tissue incubated with a mixture of glucose, palmitate, and glutamine showed a robust reduction in coupling ratios due to increased basal

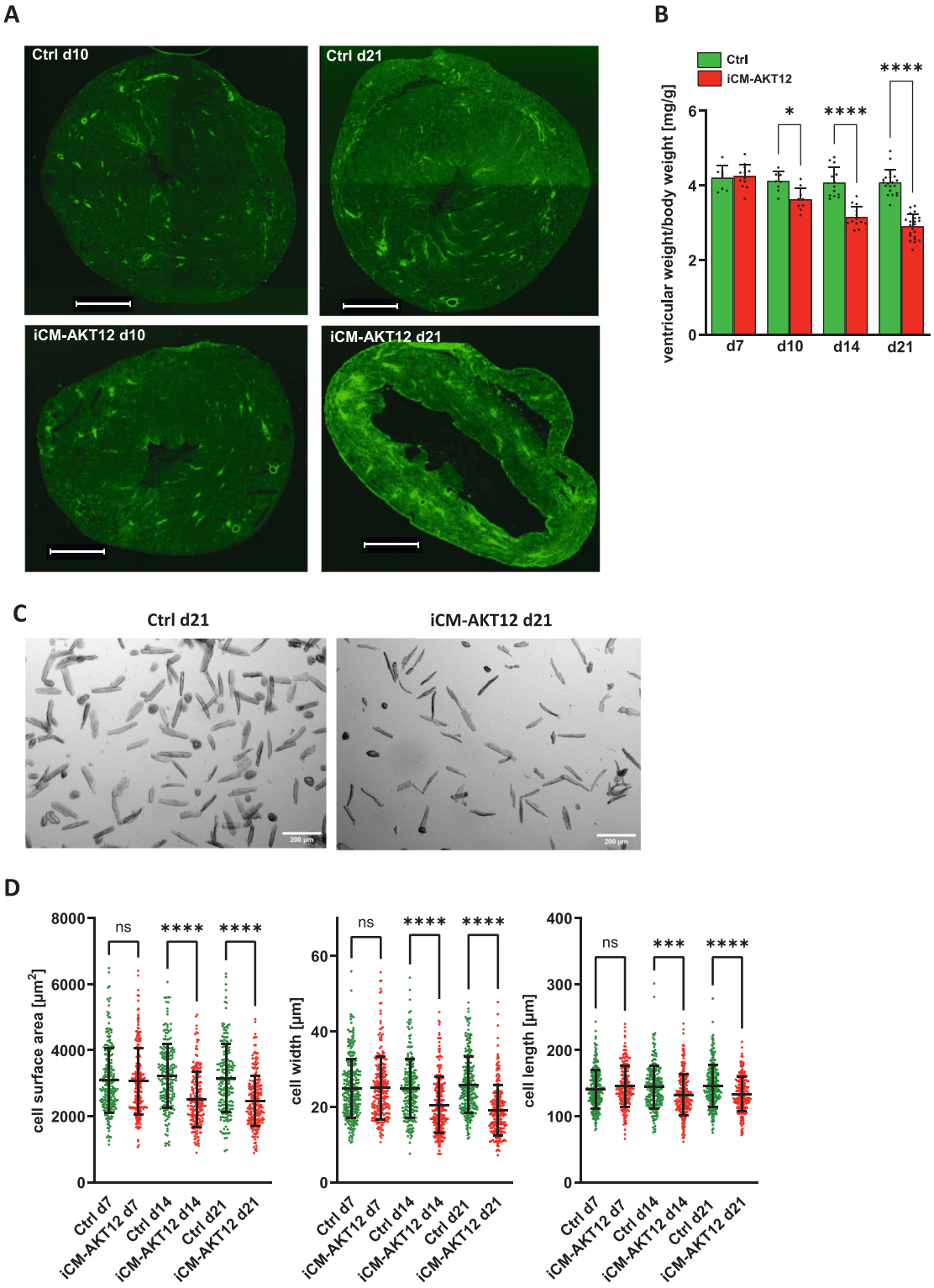

Fig. 2. Combined AKT deletion induces cardiac cellular atrophy.
A: WGA-FITC staining of heart tissue sections of Ctrl ($Ctrl^{Cre+}$) and KO (iCM-AKT12) hearts on d10 and d21 after first OH-Txf injection. Scale bars represent 1000 µm.
B: Ventricular weight to body weight ratio of Ctrl ($Ctrl^{Cre+}$) and KO (iCM-AKT12) mice at different time points. Statistical analysis was performed using two-way ANOVA followed by Šidák's multiple comparison test to compare Ctrl vs. KO at each point of time. n = 9–27, *p < 0.05, ****p < 0.0001.
C: Representative images of isolated cardiomyocytes from one Ctrl ($Ctrl^{Cre+}$) and one KO (iCM-AKT12) mouse isolated on d21. Scale bars represent 200 µm.
D: Cell surface area, cell width, and cell length of isolated cardiomyocytes from Ctrl ($Ctrl^{Cre+}$; green dots) and KO (iCM-AKT12; red dots) (n = 4 per group). A minimum of 50 individual cells per heart were measured. Statistical analysis was performed using two-way ANOVA followed by Šidák's multiple comparison test to compare Ctrl vs. KO at each point of time. *** p < 0.001, ****p < 0.0001. (For interpretation of the references to colour in this figure legend, the reader is referred to the web version of this article.)

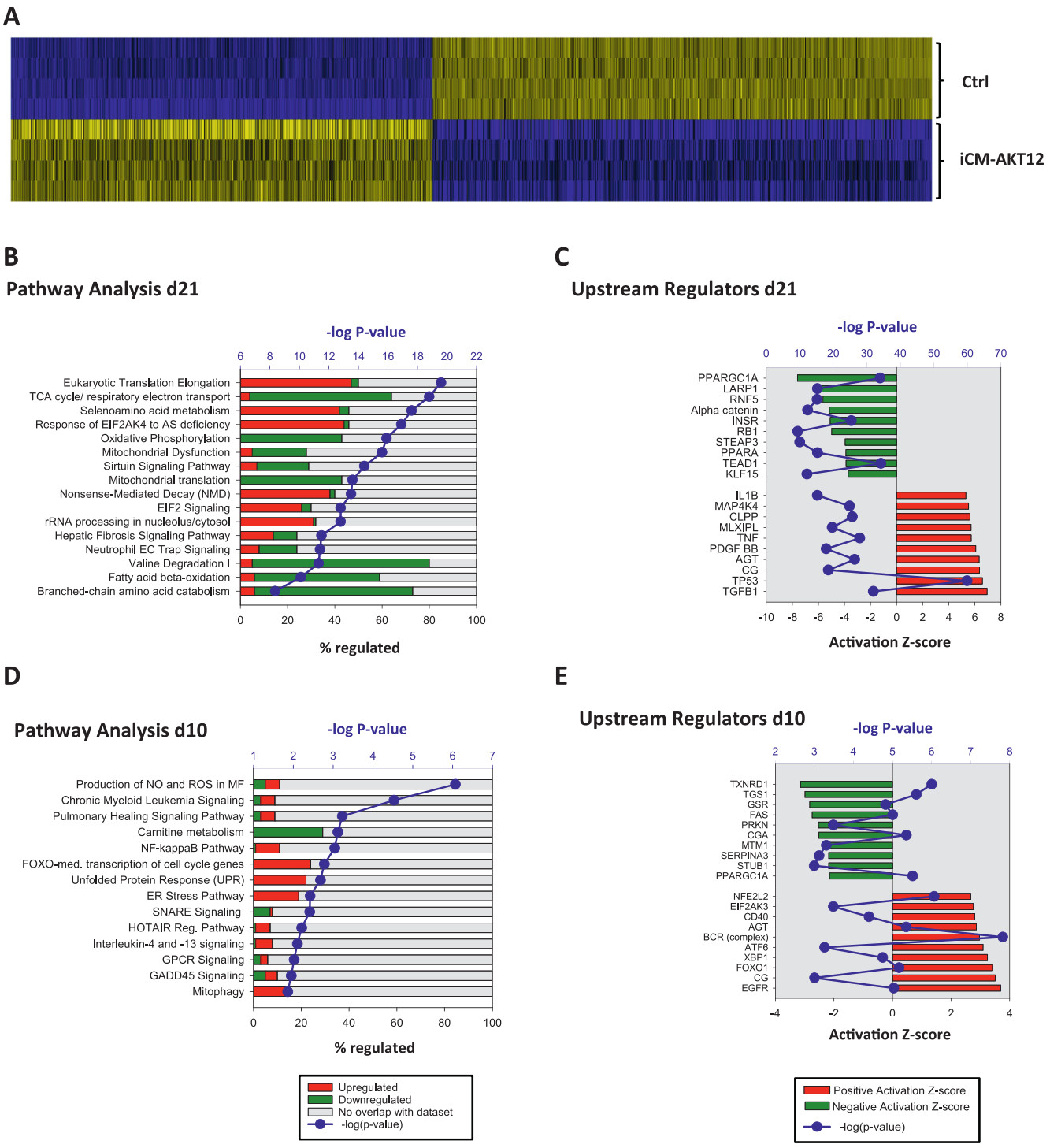

Fig. 3. AKT deletion induces down-regulation of mitochondrial gene expression.
A: Hierarchical cluster analysis of differentially expressed genes in hearts of Ctrl ($Ctrl^{Cre+}$) versus KO (iCM-AKT12) mice on d21 (n = 4 per genotype; FC ≥ 1.5, p < 0.01).
B, D: Canonical pathways identified by Ingenuity Pathway Analyses (IPA) of genes differentially expressed on d21 (B) and d10 (D). Blue dots: -log p values of regulation. Stacked bars: percentage of regulated genes (green: downregulated; red: upregulated).
C, E: IPA of upstream regulators of differential gene expression on d21 (C) and d10 (E). Upstream regulators with absolute activation *Z*-score ≥ 4, -logP≥8 (d21) or absolute activation Z-score ≥ 2, -logP≥2 (d10) are shown. (For interpretation of the references to colour in this figure legend, the reader is referred to the web version of this article.)

OCRs in combination with moderately increased uncoupled OCR values after administration of the mitochondrial uncoupler FCCP as compared to control tissue, indicating a general metabolic dysfunction (Supplemental Table 9). The contribution of the three substrates to maximal respiration was determined by measuring the decline of oxygen consumption after administration of inhibitors for the metabolism of either long chain FA (etomoxir), glucose (UK5099), or glutamine (BPTES). The dependency on a specific substrate was expressed in percent of all

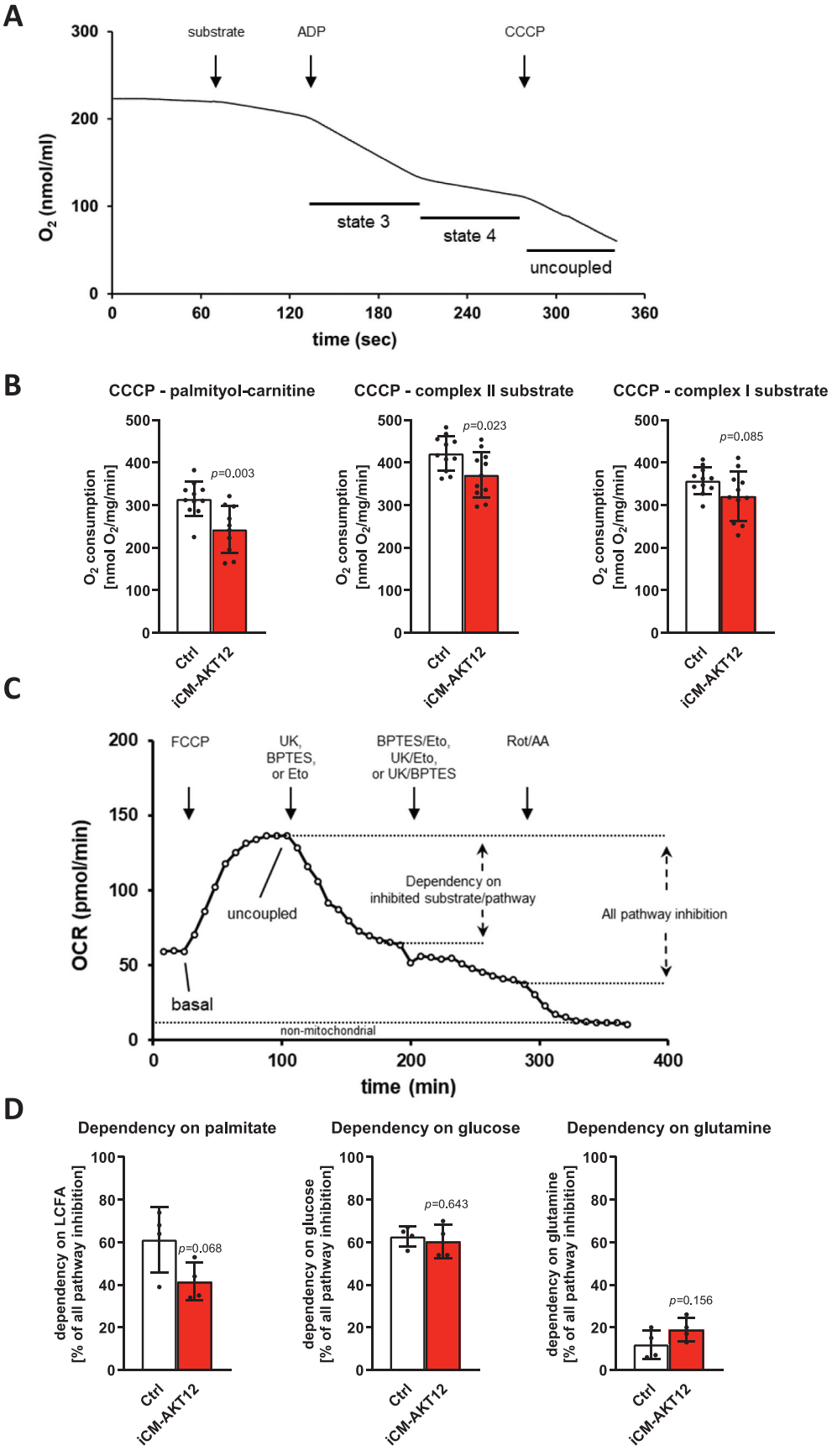

(caption on next page)

Fig. 4. Combined AKT deletion impairs cardiac metabolism.
A: Representative trace of mitochondrial respiration measurements. Respiration was initiated by the addition of substrate; state 3 respiration was initiated by the addition of ADP. After reaching stable state 4 respiration, uncoupling was achieved by the addition of CCCP (Carbonyl cyanide-*m*-chlorophenylhydrazone).
B: Uncoupled mitochondrial O_2 consumption using different substrates (n = 10–11 mitochondrial preparations, d21), Ctrl = $Ctrl^{Cre+}$, KO = iCM-AKT12.
C: Representative registration of oxygen consumption rate (OCR) measurement of intact cardiac tissue for investigation of substrate pathway dependencies by using different inhibitors. Basal respiration in DMEM (palmitate/glucose/glutamine) was determined prior to the addition of carbonyl cyanide-*p*- trifluoromethoxyphenylhydrazone (FCCP) for mitochondrial uncoupling. UK5099, BPTES, or etomoxir (ETO) was added for the inhibition of glucose, glutamine, or palmitate utilization, respectively, to determine the dependency of the inhibited pathway. Addition of the two other inhibitors allowed to determine the effect of inhibition of all pathways. Non-mitochondrial oxygen consumption was determined after electron transport chain inhibition by rotenone (rot) and antimycin A (AA).
D: Quantification of the dependency of Ctrl ($Ctrl^{fl/fl}$) and KO (iCM-AKT12) heart tissue (d21) on palmitate, glucose, or glutamine (n = 4 independent organ preparations per genotype, 4 tissue slices per organ). Dependencies on the given substrate are determined as OCR after selected pathway inhibition normalized to OCR after all pathway inhibition.
Ctrl = white bars, iCM-AKT12 = red bars. Data represent means ± SD. Statistical analyses were performed using unpaired, two-tailed Student's *t*-test. (For interpretation of the references to colour in this figure legend, the reader is referred to the web version of this article.)

pathway inhibition, measured by subsequent administration of the respective other inhibitors (Fig. 4C, Supplemental Table 9). The dependency on long chain FA was strongly reduced by 30% in iCM-AKT12 tissue, whereas glucose dependency was not affected, and glutamine dependency tended to be increased (Fig. 4D). The ability to utilize substrates depends largely on the import of substrates into cells or mitochondria. We therefore investigated the expression of key transporters for the above used substrates. In accordance with the reduced FA dependency, expression of the mitochondrial LCFA import proteins CPT1b and CPT2 was significantly reduced in iCM-AKT12 hearts (Fig. S6D). We further observed a strong upregulation of the constitutive glucose transporter GLUT1, whereas expression of the AKT-regulated glucose transporter GLUT4 was not altered (Fig. S6E). Finally, transcription of *Slc1a5* and *Slc38a2* both encoding neutral amino acid transporters capable of importing glutamine into the cell was increased in iCM-AKT12 hearts (Fig. S6F), and Slc38a2 was among the most highly upregulated proteins detected in the proteome analysis of d21 hearts (Fig. S8B). In order to investigate the systemic supply of substrates to the heart, blood glucose, plasma ß-hydroxybutyrate (ß-OH), and plasma NEFA levels on d14 and d21 were measured in control and KO mice. There were no differences in blood glucose, a trend towards reduced NEFA levels on d21, and decreased ß-OH levels on d14 and d21 in KO mice (Fig. S2H).

Next, we investigated whether metabolic functional impairment led to energetic limitation of cardiac tissue in vivo. Repetitive, volume-selective ^{31}P-MR spectroscopy was performed with control and KO mice to quantify ATP and phosphocreatine (PCr) levels in left ventricles. Representative cardiac MR spectra of one individual KO mouse

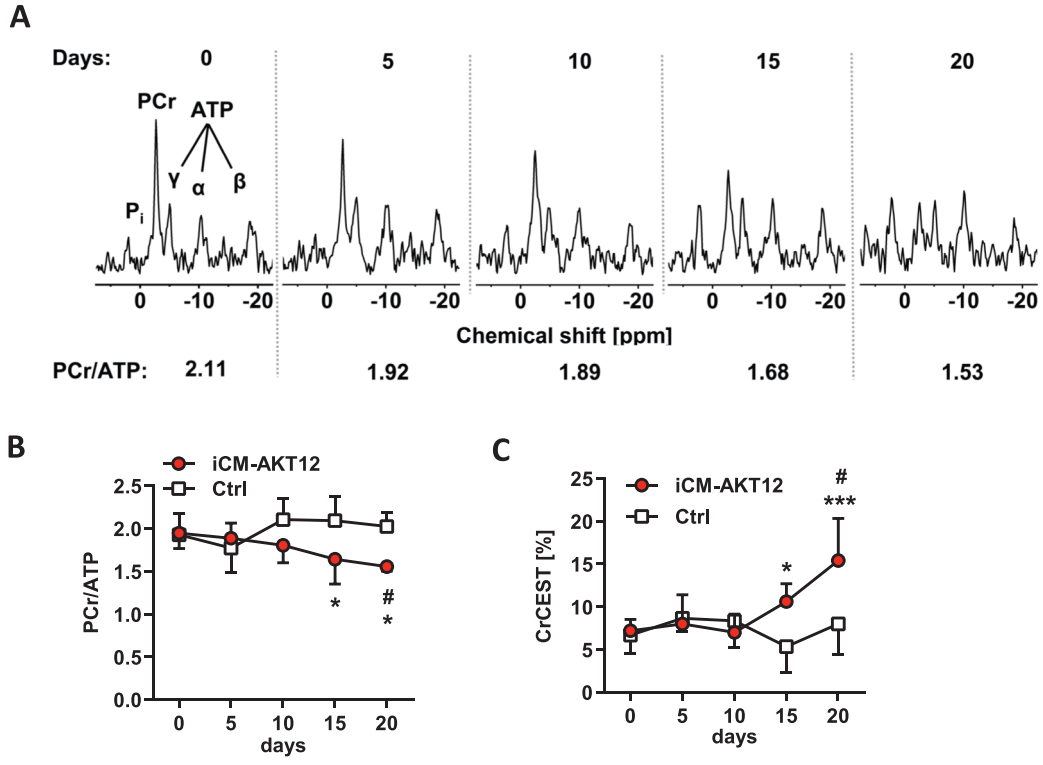

Fig. 5. Cardiac magnetic resonance (MR) demonstrates successive high-energy phosphate depletion in iCM-AKT12 hearts.
A: Representative cardiac ^{31}P MR spectra extracted from 2D ^{31}P chemical shift imaging (CSI) data sets of an individual KO (iCM-AKT12) mouse recorded before (d0) and on day 5, 10, 15 and 20 after induction of KO. Each phosphorous atom yields a unique signal; PCr, phosphocreatine; ATP, adenosine triphosphate; P_i, inorganic phosphate. Note the continuously decreasing PCr and increasing P_i signals over time, indicating failing PCr resynthesis.
B: Quantification of cardiac PCr/ATP ratios in KO mice (iCM-AKT12; n = 5) and Ctrl mice ($Ctrl^{Cre+}$; n = 3) over the observation period.
C: In parallel to declining PCr levels, increasing cardiac creatine formation was detected by CrCEST (creatine chemical exchange saturation transfer) in KO mice (n = 5) compared to Ctrl mice (n = 3).
Data represent means ± SD. Statistical analyses were performed using two-way ANOVA (RM) followed by Tukey's multiple comparison test to compare Ctrl versus KO at each point of time (*p ≤ 0.05, ***p ≤ 0.001) or alterations in the individual genotypes compared to basal values (d0) ($^{\#}$p ≤ 0.05).

demonstrated progressive reduction of cardiac energetics as evident by the gradual decline of the PCr peak (Fig. 5A), resulting in reduction of the PCr/ATP ratio from 2.1 before first OH-Txf injection (d0) to 1.5 on d20 (Fig. 5B). The decline was accompanied by a rise in free creatine levels as measured by CrCEST imaging (Fig. 5C). Interestingly, we observed a significant reduction in transcription of the genes *Ckm* and *Ckmt2* encoding cytosolic and mitochondrial creatine kinase, respectively (Fig. S6G). This could also have an impact on cardiac energy supply.

Taken together, metabolic and mitochondrial dysfunction with the restriction of FA utilization lead to progressive cardiac energy depletion in iCM-AKT12 mice.

3.6. Fatty acid metabolites accumulate in iCM-AKT12 hearts

To investigate the impact of the depressed lipid metabolism on cardiac lipid composition, we used the Biocrates AbsoluteIDQ® p180 system and LC-MS/MS for detection of lipid metabolites in heart tissues on d14 and d21. As shown in Fig. 6A, d21 but not d14 KO hearts showed a significant increase in the acylcarnitines (AC)/carnitine (C0) ratio that was due to an accumulation of numerous acylcarnitine species rather than to a decrease in free carnitine (Fig. 6B in fold change; Supplemental

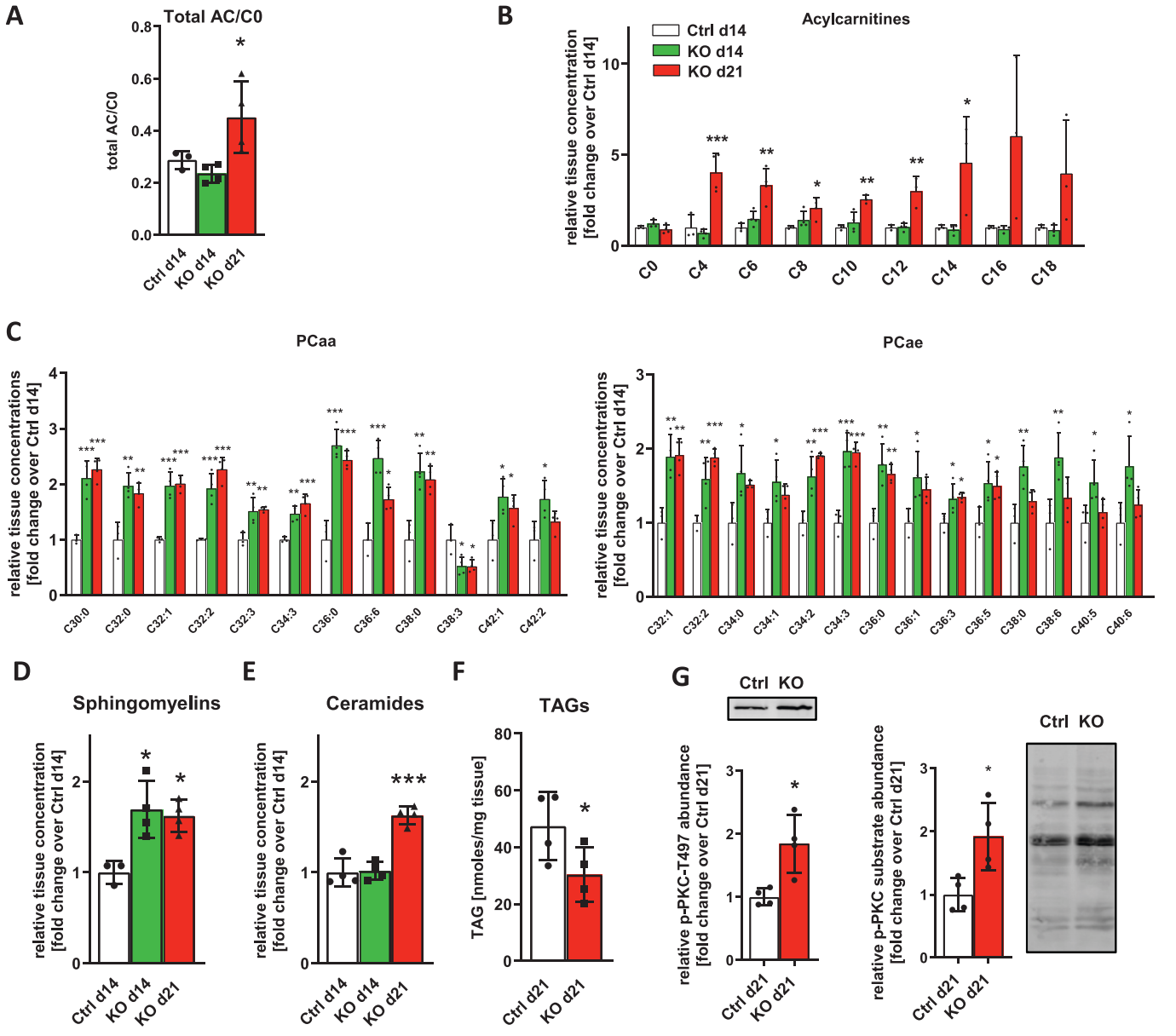

Fig. 6. Altered lipid metabolism leads to the accumulation of lipid metabolites in iCM-AKT12 hearts.
A, B, C, D, E: Lipid profiles from heart tissues of Ctrl ($Ctrl^{Cre+}$) mice on d14 (white bars, n = 3) and KO (iCM-AKT12) mice on d14 (green bars, n = 4) and d21 (red bars, n = 4). (A): ratio of total acylcarnitines (AC) to carnitine (C0). Tissue concentrations of (B): individual acylcarnitines, (C): diacyl-phosphatidylcholines (PCaa) and acyl-alkyl-phosphatidylcholines (PCae), (D): sphingomyelins, and (E): ceramides were normalized to Ctrl d14 values. Data represent mean ± SD, one-way ANOVA followed by Dunnett's multiple comparisons test was used for comparison of Ctrl d14 vs. KO d14 or KO d21. *p ≤ 0.05, **p ≤ 0.01, ***p ≤ 0.001.
F: Triacyl-glycerol (TAG) content in cardiac tissues of Ctrl ($Ctrl^{Cre+}$, white bar) and KO (iCM-AKT12, red bar) mice on d21. Data represent mean ± SD, unpaired, two-tailed *t*-test, *p ≤ 0.05 (n = 4).
G: Phosphorylations of protein kinase C on threonine 497, and PKC substrates in cardiac tissue from Ctrl ($Ctrl^{fl/fl}$) and KO mice on d21. Data represent mean ± SD, unpaired, two-tailed *t*-test, *p ≤ 0.05 (n = 4). (For interpretation of the references to colour in this figure legend, the reader is referred to the web version of this article.)

Table 10 in pmoles/mg tissue). For example, butyryl- (C4), myristoyl- (C14), palmitoyl- (C16), and stearoyl-carnitine (C18) were increased 4–6 fold over control levels. In addition, various diacyl-phosphatidylcholines (PCaa) and acyl-alkyl- phosphatidylcholines (PCae) were increased in d14 and d21 KO heart tissue (Fig. 6C, Supplemental Table 11). In particular, the content of saturated FA in phosphatidylcholines was elevated, resulting in reduced ratios of mono- or polyunsaturated FA/saturated FA in KO hearts (Fig. S9). Along the same line, sphingomyelins (Fig. 6D, Supplemental Table 12) and ceramides were increased in KO hearts (Fig. 6E). In detail, cardiotoxic ceramides including ceramides with C16, C24, or C24:1 fatty acid residues were significantly elevated (Supplemental Table 13). Cardiomyocytes can dispose excess FA by formation of triacyl-glycerol (TAG) in the endoplasmic reticulum (ER) and storage in lipid droplets (LD) to avoid accumulation of toxic lipid metabolites. Notably, despite of the high load of lipid intermediates, TAG levels were reduced in d21 iCM-AKT12 hearts (Fig. 6F).

Taken together, iCM-AKT12 hearts accumulate a broad spectrum of lipid species, including cardiotoxic lipids and lipids with potential signaling function. One mechanism of lipotoxicity in the heart is the activation of signaling pathways like for example protein kinase C signaling [32]. In fact, we found enhanced activating phosphorylation of PKC-α at T479 and elevated abundance of phosphorylated PKC substrates in iCM-AKT12 hearts (Fig. 6G).

3.7. Lipid droplet homeostasis is disturbed in iCM-AKT12 hearts

Perilipins are lipid droplet associated proteins with important structural and regulatory function in TAG storage and release. As we had identified perilipins PLIN2 and PLIN5 among the most downregulated proteins in the proteomic analysis of d21 iCM-AKT12 hearts, we next investigated the expression of cardiac perilipins at earlier time points by performing combined Western blot (Fig. 7A) and qPCR analyses (Fig. 7B). We observed an early onset (d7) reduction of PLIN2 protein but no decrease in *Plin*2 mRNA level, suggesting early post-transcriptional reduction of PLIN2 by protein degradation. *Plin*3 mRNA expression was increased on d7 and d10, whereas PLIN3 protein remained stable, suggesting that PLIN3 might also be reduced post-transcriptionally. Perilipin 5 expression was reduced early and progressively, both on the level of mRNA and protein. Moreover, we found reduced mRNA expression of *Lpin1 (*2.5 fold), *Fitm1 (*4.2 fold), and *Dgat2 (*3.1 fold), all involved in LD formation (Fig. S6H).

To investigate the capacity of LD formation, cardiomyocytes from control and iCM-AKT12 hearts were isolated at different time points and cultivated overnight with oleic acid to induce LD formation. Confocal PLIN2 and PLIN5 immunofluorescence microscopy clearly showed a lower LD density in KO cardiomyocytes (Fig. 7C). For quantification of LD density we used PLIN3 labelling (Fig. S10A), as PLIN3 protein levels were only moderately reduced in iCM-AKT12 hearts, and found that LD density was progressively reduced (Fig. 7D). Next, we analyzed LD in heart tissue sections of mice starved overnight to induce cardiac LD formation. Double staining for either PLIN2 and PLIN5 or PLIN2 and PLIN3 revealed double-positive, punctate signals in control hearts, presumably representing LD. Although there appeared to be a higher density of LD in non-cardiomyocyte cells, we detected LD in the cytoplasm of cardiomyocytes as well. In contrast, in KO hearts, LD signals were almost exclusively located in non-cardiomyocytes, while the cytoplasm of cardiomyocytes was almost devoid of punctate signals (Fig. S10 B,C).

4. Discussion

Cardiomyocyte structural and functional integrity is a fundamental prerequisite for a proper long-term function of these long-lived, terminally differentiated cells. In particular, the maintenance of sustained energetic supply is essential to preserve cardiomyocyte function even under conditions of changing workload. The strictly aerobic cardiomyocytes depend on the supply of substrates and on mitochondrial respiration to generate sufficient energy to maintain contractile activity, ion homeostasis, and functional cellular structures.

The insulin-PI3K-AKT signaling axis plays a fundamental role in the control of cell growth and metabolism, and malfunctions relate to various pathologies like insulin resistance, type 2 diabetes, or obesity. To address the impact of AKT signaling on the function of the adult heart, we simultaneously inactivated the major AKT isoforms AKT1 and AKT2 in cardiomyocytes of the adult mouse (iCM-AKT12). Here we demonstrate that AKT function is indispensable for the control of adult cardiomyocyte homeostasis and, in particular, FA metabolism and mitochondrial function. Simultaneous deletion of both isoforms caused a rapidly progressive and lethal heart failure due to pronounced cardiomyocyte atrophy, metabolic remodeling, mitochondrial dysfunction, energetic depletion, and extensive alterations in cardiac gene expression. In contrast, the inducible deletion of either AKT1 (iCM-AKT1) or AKT2 (iCM-AKT2) alone displayed normal basic parameters of heart function as well as general condition and behavior. This finding indicates that the activity of each individual isoform was sufficient to provide the maintenance of essential homeostatic AKT functions in the myocardium, underlining redundant roles of AKT1 and AKT2 in the non-stressed heart. Accordingly, phosphorylation of canonical AKT targets was reduced in the single KO in comparison to control hearts, but was substantially lower in iCM-AKT12 hearts, indicating an additive action of both isoforms on the same phosphorylation targets. In a previous report, inducible cardiomyocyte-restricted deletion of AKT2 in mice with germline AKT1 knockout led to a moderate cardiac phenotype with reduced contractility, no signs of cardiac atrophy or reduced survival, but reduced expression of the gap junction protein connexin43 (Cx43) [13]. This differs significantly from the iCM-AKT12 model, which developed a much more severe heart failure and no reduction in Cx43 expression. Reasons for the different phenotypes could lie in the genetic model. Germline inactivation of the AKT1 gene could have led to compensatory adaptation and thus to a mitigated phenotype in the other model.

In iCM-AKT12 mice, induced inactivation of the central signaling hub AKT resulted in a highly complex cardiac phenotype. This complicates the differentiation of primary, directly AKT-dependent effects from secondary processes caused by primary malfunctions and rewiring of parallel and downstream signaling mechanisms. One of the earliest changes was a selective and progressive reduction of myocardial perilipins PLIN5, PLIN2 and PLIN3, which – at least in the case of PLIN2 - was not attributable to reduced transcription. PLIN2 stabilizes LD and shields the stored lipids from lipolysis [33]. Under nutrient deprivation, PLIN2 is degraded, followed by degradation of LD [34]. PLIN5 acts as a lipolytic barrier to prevent unregulated lipolysis. Following PKA-mediated phosphorylation, inhibition of lipolysis by PLIN5 is reversed and TAG are hydrolyzed [35]. PLIN3 has been described to be involved in the early stage of LD biogenesis and is used as a marker to detect nascent LD [36,37].

It is well described that the AKT/mTOR pathway negatively regulates autophagy in many systems including the heart [26,27]. Lipophagy is a special form of macroautophagy, in which LD are degraded by the autophagic machinery of the cell. Before being degraded in the lysosome, LD might be reduced in size by lipolysis and chaperone-mediated autophagy (CMA). CMA targets specific proteins for selective lysosomal degradation [38] and can be triggered by cellular stress such as starvation [39]. PLIN2, PLIN3, and PLIN5 have been reported to be substrates for CMA in murine livers and cultivated cells [34] [40]. The selective, transcription-independent decrease of PLIN2 and potentially also of the other CMA substrates PLIN3 and PLIN5 in iCM-AKT12 hearts preceded a detectable increase in macroautophagy, indicated by an increased expression of key autophagic factors like Bnip3 or Sqstm1/p62. This suggests that the loss of perilipins might be due to a selective degradation process like CMA rather than the consequence of lipophagy

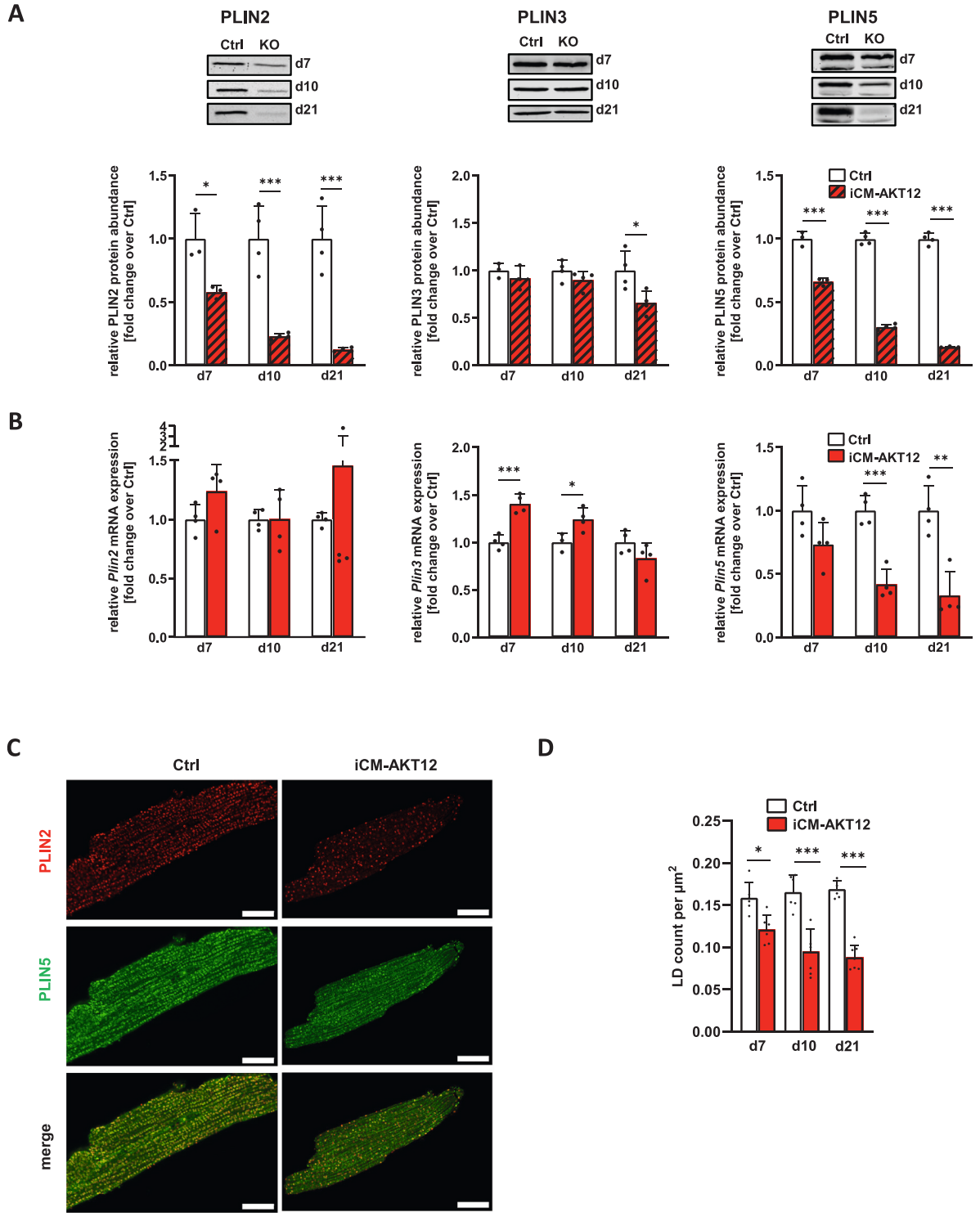

Fig. 7. Impaired perilipin expression and lipid droplet formation in iCM-AKT12 hearts.
A, B: Time course of perilipin gene expression in cardiac tissue of Ctrl ($Ctrl^{fl/fl}$) and KO (iCM-AKT12) mice (n = 4). A: Protein abundance (Western blot), B: RNA expression (qPCR). Data are normalized to Ctrl expressions at the given point of time and represent mean ± SD. Unpaired, two-tailed Student's *t*-test was used to compare Ctrl vs. KO at each point of time. *p ≤ 0.05, **p ≤ 0.01, ***p ≤ 0.001.
C: Lipid droplet (LD) immunofluorescence staining in Ctrl ($Ctrl^{fl/fl}$) and KO (iCM-AKT12) cardiomyocytes isolated on d21 after start of KO induction and cultured in the presence of oleic acid to induce LD formation. PLIN2 is shown in red, PLIN5 is shown in green (Magnification x630, scale bars = 20 µm).
D: Quantification of LD density in oleic acid exposed cardiomyocytes of Ctrl ($Ctrl^{fl/fl}$) and KO (iCM-AKT12) hearts isolated at different points of time. LD density was counted in confocal images of at least 3 individual cardiomyocytes from two different preparations per time and genotype. Two-way ANOVA followed by Šidák's multiple comparison test was used to compare control vs. KO at each point of time. *p ≤ 0.05, ***p ≤ 0.001. (For interpretation of the references to colour in this figure legend, the reader is referred to the web version of this article.)

of the entire LD. Lysosomal AKT was reported to suppress CMA in both mouse fibroblasts and rat liver tissue [41]. However, only a limited number of studies have examined the relevance of CMA in cardiac tissue [42] [43]. Our observations could provide substantial evidence for CMA-mediated induction of lipophagy in the stressed mouse heart. Based on our timeline study of perilipin expression, we propose that the upregulation of *Plin3* transcription in the early phase indicates an initial increase in LD biogenesis that seemed to be rapidly counteracted by degradation processes, leading to reduced perilipin abundancies, potentially by CMA. Later, the ability to synthesize new LD seemed to be impaired due to reduced expression of genes related to LD biogenesis, such as *Lpin1*, *Dgat2*, or *Fitm1*. As a result, LD formation in isolated knockout cardiomyocytes fed with oleate was increasingly limited, and LD were undetectable in cardiomyocytes in iCM-AKT12 heart tissue sections. Obviously, AKT deletion drastically reduced the capacity of cardiomyocytes to store excess fatty acids in a harmless form, thereby contributing to cardiomyocyte stress.

The increasing heart failure induced by AKT deletion was accompanied by global changes in cardiac gene expression. The most striking alteration in the transcriptome of iCM-AKT12 hearts was the concerted downregulation of canonical pathways related to mitochondrial function, e.g. β-oxidation, the TCA cycle, and oxidative phosphorylation. In line with this, bioinformatic analysis identified PGC-1α, the master regulator of mitochondrial biogenesis, as downregulated. Given the lack of reduction in the amount of PGC-1α protein, we postulate an inhibition of PGC-1α at the post-translational level. Reports in the literature on a modulation of PGC-1α activity by AKT are ambiguous [44]. In cultivated cells, AKT can phosphorylate and thereby inactivate PGC-1α [45,46]. Consequently, the deletion of AKT would increase rather than inhibit PGC-1α activity. The extensive early depression in PLIN5 protein levels may be a key linking loss of AKT to a reduction of PGC-1α activity. It was demonstrated that under conditions of starvation PLIN5 migrates to the nucleus, where it can promote PGC-1α mediated expression of genes involved in mitochondrial biogenesis and oxidative function [47,48]. Early loss of PLIN5 due to degradation could therefore contribute to the suppression of PGC-1α activity in iCM-AKT12 hearts.

AKT is well described as a regulator of glucose metabolism in insulin-sensitive tissue. Surprisingly, glucose utilization was largely preserved upon AKT deletion in our experimental approach. Upregulation of the constitutive glucose transporter GLUT1 most likely compensated a reduced glucose uptake via GLUT4. However, our experimental data obtained by a combination of complementary metabolic and molecular analyses demonstrated that fatty acid (FA) metabolism was substantially impaired in iCM-AKT12 hearts. Mitochondrial respirometry uncovered that in mitochondria from d21 hearts the oxidation of FA was particularly compromised (−30%), whereas glutamate/malate and succinate dependent oxidation were only mildly reduced (−10%). In addition, iCM-AKT12 mitochondria developed a general, substrate-independent attenuation of mitochondrial efficiency, as P/O ratios were reduced for all substrates tested. On the tissue level, extracellular flux measurements of cardiac tissue slices showed an enhanced basal and uncoupled OCR as well as reduced coupling ratios upon AKT deletion, indicating a general metabolic malfunction. FA dependency, defined as the relative portion of FA mediated mitochondrial oxidation that cannot be compensated by utilization of other fuels, was most strongly impaired. Glucose dependency, however, was not altered, and glutamine dependency slightly increased in iCM-AKT12 heart tissue, suggesting a rewiring of substrate utilization. Transcriptomic and proteomic data underlined that the AKT1/2 deletion particularly affected cardiomyocyte FA utilization. A reduction in protein levels of the carnitine shuttle and β-oxidation most likely contributed to the limited mitochondrial FA oxidation capacity. The early reduction of PLIN5 could have a direct influence on mitochondrial function as well. It has been shown that LD-bound PLIN5 can form contact sites to mitochondria, thus enhancing FA trafficking and β-oxidation [49]. Moreover, coupling of LD to mitochondria via PLIN5 increases mitochondrial respiratory capacity [50].

Taken together, combined AKT1 and AKT2 deficiency in the heart promoted a reduced FA oxidative capacity. This probably contributed significantly to the pronounced energetic depletion that was observed by in vivo NMR studies on beating hearts. Cardiac PCr/ATP ratio dropped from a normal value of 2 (d0) below 1.6 (d20), a value typically found in severe heart failure in humans [51,52]. A concomitant rise in creatine concentrations in the myocardium, which was detectable from d10 after KO induction, underscored the compromised cardiac energetics.

In terms of pathomechanism, the reduced mitochondrial lipid oxidation, combined with the release of fatty acids by autophagy, and a compromised synthesis and storage capacity of triacylglycerols in LD led to the accumulation of potentially harmful lipid metabolites in iCM-AKT12 heart tissue. Acylcarnitine accumulation and redirection of lipids towards ceramide and sphingomyelin formation might cause lipotoxicity and cellular stress in various ways [32,53]. Myocardial accumulation of long-chain acylcarnitines inhibits mitochondrial oxidation [54], and accumulation of long chain acyl-CoA in the myocardium is the metabolic hallmark of human diabetic cardiomyopathy [55]. Elevated concentrations of ceramides can lead to activation of PKC [56], and an enhanced PKC activity has been observed under various pathological conditions in the heart [57], including in iCM-AKT12 hearts in this study. Moreover, ceramides have been associated with inhibition of the mitochondrial electron transport chain in skeletal muscle cells [58] and therefore may contribute to mitochondrial dysfunction in iCM-AKT12 hearts as well. In addition, the reduced ratios of mono- and polyunsaturated FA/saturated FA in membrane lipids might cause reduced membrane fluidity and cell damage.

In this study, we could show that AKT is essential for cellular homeostasis of adult cardiomyocytes. Whereas AKT and in particular AKT2 is predominantly linked to the insulin-glucose axis, we find that in the heart, AKT1 and AKT2 are particularly important for FA metabolism, as AKT deletion led to increased breakdown of intracellular lipid stores, impaired capacity to utilize fatty acids, and eventually an accumulation of fatty acid intermediates and lipotoxicity. Since the earliest alteration we observed was the loss of perilipins and LD, we hypothesize that the early disturbance of FA metabolism is a major pathomechanism contributing to if not initializing heart failure development in iCM-AKT12 mice.

We are aware that the iCM-AKT12 knockout is an extreme and complex model system, which in a comparable manner does not occur in humans and has therefore a limited direct transferability to human heart disease. In addition, we presently only have limited data on sex-specific differences in iCM-AKT12 mice, but at least cardiac atrophy occurs to a similar extent in females as in males. Therefore, we assume that similar pathomechanisms are activated in female iCM-AKT12 hearts. iCM-AKT12 mice, however, represent a highly interesting model system for basic research studies analyzing cardiac signaling networks, as it allows uncovering of novel regulatory mechanisms that might contribute to human diseases such as diabetic cardiomyopathy (DCM) as well. The complex phenotype complicates the identification of early and primarily AKT-mediated effects, but the data presented in this study imply that AKT and therefore insulin-dependent signaling is a major regulator of cardiac lipid metabolism. Despite some limitations, the results presented here warrant further investigation into the role of AKT, CMA, and perilipins in cardiac disorders.

CRediT authorship contribution statement

Stefanie Gödecke: Writing – original draft, Investigation, Formal analysis, Data curation, Conceptualization. **André Heinen:** Writing – review & editing, Writing – original draft, Investigation. **Tim Appel:** Investigation. **Phil-Torben Müller:** Investigation. **Tim Stemmer:** Investigation. **Daniela Müller:** Investigation. **Uli Flögel:** Writing – original draft, Investigation, Formal analysis. **Diran Herebian:** Investigation, Formal analysis, Data curation. **Fiorella A. Solari:** Writing –

original draft, Investigation, Formal analysis. **Rene Deenen:** Investigation, Formal analysis. **Karl Köhrer:** Investigation, Formal analysis. **Albert Sickmann:** Supervision. **Axel Gödecke:** Writing – review & editing, Writing – original draft, Validation, Supervision, Funding acquisition, Data curation.

Declaration of competing interest

The authors declare that they have no known competing financial interests or personal relationships that could have appeared to influence the work reported in this paper.

Acknowledgements

This work was funded by Deutsche Forschungsgemeinschaft (DFG) CRC1116 Grant No: 236177352, Project A06 (AG) and Project S01 (AS and AG), and by a grant from Dr. Sigrid-Worch-Pöhler-Stiftung, Düsseldorf (AG).

Appendix A. Supplementary data

Supplementary data to this article can be found online at https://doi.org/10.1016/j.metabol.2026.156619.

References

[1] Sadek H, Olson EN. Toward the goal of human heart regeneration. Cell Stem Cell 2020;26:7–16. https://doi.org/10.1016/j.stem.2019.12.004.
[2] Vega RB, Horton JL, Kelly DP. Maintaining ancient organelles: mitochondrial biogenesis and maturation. Circ Res 2015;116:1820–34. https://doi.org/10.1161/circresaha.116.305420.
[3] Kolwicz Jr SC, Purohit S, Tian R. Cardiac metabolism and its interactions with contraction, growth, and survival of cardiomyocytes. Circ Res 2013;113:603–16. https://doi.org/10.1161/circresaha.113.302095.
[4] Nakamura M, Sadoshima J. Cardiomyopathy in obesity, insulin resistance and diabetes. J Physiol 2020;598:2977–93. https://doi.org/10.1113/jp276747.
[5] Walsh K. Akt signaling and growth of the heart. Circulation 2006;113:2032–4. https://doi.org/10.1161/circulationaha.106.615138.
[6] Reinartz M, Raupach A, Kaisers W, Gödecke A. AKT1 and AKT2 induce distinct phosphorylation patterns in HL-1 cardiac myocytes. J Proteome Res 2014;13:4232–45. https://doi.org/10.1021/pr500131g.
[7] Cho H, Thorvaldsen JL, Chu Q, Feng F, Birnbaum MJ. Akt1/PKBalpha is required for normal growth but dispensable for maintenance of glucose homeostasis in mice. J Biol Chem 2001;276:38349–52. https://doi.org/10.1074/jbc.C100462200.
[8] DeBosch B, Treskov I, Lupu TS, Weinheimer C, Kovacs A, Courtois M, et al. Akt1 is required for physiological cardiac growth. Circulation 2006;113:2097–104. https://doi.org/10.1161/circulationaha.105.595231.
[9] Cho H, Mu J, Kim JK, Thorvaldsen JL, Chu Q, Crenshaw 3rd EB, et al. Insulin resistance and a diabetes mellitus-like syndrome in mice lacking the protein kinase Akt2 (PKB beta). Science 2001;292:1728–31. https://doi.org/10.1126/science.292.5522.1728.
[10] DeBosch B, Sambandam N, Weinheimer C, Courtois M, Muslin AJ. Akt2 regulates cardiac metabolism and cardiomyocyte survival. J Biol Chem 2006;281:32841–51. https://doi.org/10.1074/jbc.M513087200.
[11] Peng XD, Xu PZ, Chen ML, Hahn-Windgassen A, Skeen J, Jacobs J, et al. Dwarfism, impaired skin development, skeletal muscle atrophy, delayed bone development, and impeded adipogenesis in mice lacking Akt1 and Akt2. Genes Dev 2003;17:1352–65. https://doi.org/10.1101/gad.1089403.
[12] Wang Q, Yu WN, Chen X, Peng XD, Jeon SM, Birnbaum MJ, et al. Spontaneous hepatocellular carcinoma after the combined deletion of Akt isoforms. Cancer Cell 2016;29:523–35. https://doi.org/10.1016/j.ccell.2016.02.008.
[13] Ock S, Lee WS, Kim HM, Park KS, Kim YK, Kook H, et al. Connexin43 and zonula occludens-1 are targets of Akt in cardiomyocytes that correlate with cardiac contractile dysfunction in Akt deficient hearts. Biochim Biophys Acta Mol Basis Dis 2018;1864:1183–91. https://doi.org/10.1016/j.bbadis.2018.01.022.
[14] Heinen A, Raupach A, Behmenburg F, Hölscher N, Flögel U, Kelm M, et al. Echocardiographic analysis of cardiac function after infarction in mice: validation of single-plane long-Axis view measurements and the bi-plane Simpson method. Ultrasound Med Biol 2018;44:1544–55. https://doi.org/10.1016/j.ultrasmedbio.2018.03.020.
[15] Gödecke A, Molojavyi A, Heger J, Flögel U, Ding Z, Jacoby C, et al. Myoglobin protects the heart from inducible nitric-oxide synthase (iNOS)-mediated nitrosative stress. J Biol Chem 2003;278:21761–6. https://doi.org/10.1074/jbc.M302573200.
[16] Flögel U, Jacoby C, Gödecke A, Schrader J. In vivo 2D mapping of impaired murine cardiac energetics in NO-induced heart failure. Magn Reson Med 2007;57:50–8. https://doi.org/10.1002/mrm.21101.
[17] Readnower RD, Brainard RE, Hill BG, Jones SP. Standardized bioenergetic profiling of adult mouse cardiomyocytes. Physiol Genomics 2012;44:1208–13. https://doi.org/10.1152/physiolgenomics.00129.2012.
[18] Schindelin J, Arganda-Carreras I, Frise E, Kaynig V, Longair M, Pietzsch T, et al. Fiji: an open-source platform for biological-image analysis. Nat Methods 2012;9:676–82. https://doi.org/10.1038/nmeth.2019.
[19] Bottermann K, Kalfhues L, Nederlof R, Hemmers A, Leitner LM, Oenarto V, et al. Cardiomyocyte p38 MAPKα suppresses a heart-adipose tissue-neutrophil crosstalk in heart failure development. Basic Res Cardiol 2022;117:48. https://doi.org/10.1007/s00395-022-00955-2.
[20] Emde B, Heinen A, Gödecke A, Bottermann K. Wheat germ agglutinin staining as a suitable method for detection and quantification of fibrosis in cardiac tissue after myocardial infarction. Eur J Histochem 2014;58:2448. https://doi.org/10.4081/ejh.2014.2448.
[21] Kötter S, Kazmierowska M, Andresen C, Bottermann K, Grandoch M, Gorressen S, et al. Titin-based cardiac myocyte stiffening contributes to early adaptive ventricular remodeling after myocardial infarction. Circ Res 2016;119:1017–29. https://doi.org/10.1161/circresaha.116.309685.
[22] Heinen A, Aldakkak M, Stowe DF, Rhodes SS, Riess ML, Varadarajan SG, et al. Reverse electron flow-induced ROS production is attenuated by activation of mitochondrial Ca2+−sensitive K+ channels. Am J Physiol Heart Circ Physiol 2007;293:H1400–7. https://doi.org/10.1152/ajpheart.00198.2007.
[23] Bottermann K, Spychala A, Eliacik A, Amin E, Moussavi-Torshizi SE, Klöcker N, et al. Extracellular flux analysis in intact cardiac tissue slices-a novel tool to investigate cardiac substrate metabolism in mouse myocardium. Acta Physiol (Oxf) 2023;239:e14004. https://doi.org/10.1111/apha.14004.
[24] Thomsen R, Sølvsten CA, Linnet TE, Blechingberg J, Nielsen AL. Analysis of qPCR data by converting exponentially related Ct values into linearly related X0 values. J Bioinform Comput Biol 2010;8:885–900. https://doi.org/10.1142/s0219720010004963.
[25] Ayuso MI, Hernández-Jiménez M, Martín ME, Salinas M, Alcázar A. New hierarchical phosphorylation pathway of the translational repressor eIF4E-binding protein 1 (4E-BP1) in ischemia-reperfusion stress. J Biol Chem 2010;285:34355–63. https://doi.org/10.1074/jbc.M110.135103.
[26] Levine B, Klionsky DJ. Development by self-digestion: molecular mechanisms and biological functions of autophagy. Dev Cell 2004;6:463–77. https://doi.org/10.1016/s1534-5807(04)00099-1.
[27] Pizarro M, Troncoso R, Martínez GJ, Chiong M, Castro PF, Lavandero S. Basal autophagy protects cardiomyocytes from doxorubicin-induced toxicity. Toxicology 2016;370:41–8. https://doi.org/10.1016/j.tox.2016.09.011.
[28] Lee WS, Kim J. Peroxisome proliferator-activated receptors and the heart: lessons from the past and future directions. PPAR Res 2015;2015:271983. https://doi.org/10.1155/2015/271983.
[29] Jiao L, Liu Y, Yu XY, Pan X, Zhang Y, Tu J, et al. Ribosome biogenesis in disease: new players and therapeutic targets. Signal Transduct Target Ther 2023;8:15. https://doi.org/10.1038/s41392-022-01285-4.
[30] Ahuja P, Zhao P, Angelis E, Ruan H, Korge P, Olson A, et al. Myc controls transcriptional regulation of cardiac metabolism and mitochondrial biogenesis in response to pathological stress in mice. J Clin Invest 2010;120:1494–505. https://doi.org/10.1172/jci38331.
[31] Wang H, Yu W, Wang Y, Wu R, Dai Y, Deng Y, et al. p53 contributes to cardiovascular diseases via mitochondria dysfunction: a new paradigm. Free Radic Biol Med 2023;208:846–58. https://doi.org/10.1016/j.freeradbiomed.2023.09.036.
[32] Schulze PC, Drosatos K, Goldberg IJ. Lipid use and misuse by the heart. Circ Res 2016;118:1736–51. https://doi.org/10.1161/circresaha.116.306842.
[33] Cinato M, Andersson L, Miljanovic A, Laudette M, Kunduzova O, Borén J, et al. Role of Perilipins in oxidative stress-implications for cardiovascular disease. Antioxidants (Basel) 2024;13. https://doi.org/10.3390/antiox13020209.
[34] Kaushik S, Cuervo AM. Degradation of lipid droplet-associated proteins by chaperone-mediated autophagy facilitates lipolysis. Nat Cell Biol 2015;17:759–70. https://doi.org/10.1038/ncb3166.
[35] Pollak NM, Jaeger D, Kolleritsch S, Zimmermann R, Zechner R, Lass A, et al. The interplay of protein kinase A and perilipin 5 regulates cardiac lipolysis. J Biol Chem 2015;290:1295–306. https://doi.org/10.1074/jbc.M114.604744.
[36] Choi YM, Ajjaji D, Fleming KD, Borbat PP, Jenkins ML, Moeller BE, et al. Structural insights into perilipin 3 membrane association in response to diacylglycerol accumulation. Nat Commun 2023;14:3204. https://doi.org/10.1038/s41467-023-38725-w.
[37] Griseti E, Bello AA, Bieth E, Sabbagh B, Iacovoni JS, Bigay J, et al. Molecular mechanisms of perilipin protein function in lipid droplet metabolism. FEBS Lett 2024;598:1170–98. https://doi.org/10.1002/1873-3468.14792.
[38] Schott MB, Rozeveld CN, Weller SG, McNiven MA. Lipophagy at a glance. J Cell Sci 2022;135. https://doi.org/10.1242/jcs.259402.
[39] Tasset I, Cuervo AM. Role of chaperone-mediated autophagy in metabolism. FEBS J 2016;283:2403–13. https://doi.org/10.1111/febs.13677.
[40] Ma SY, Sun KS, Zhang M, Zhou X, Zheng XH, Tian SY, et al. Disruption of Plin5 degradation by CMA causes lipid homeostasis imbalance in NAFLD. Liver Int 2020;40:2427–38. https://doi.org/10.1111/liv.14492.
[41] Arias E, Koga H, Diaz A, Mocholi E, Patel B, Cuervo AM. Lysosomal mTORC2/PHLPP1/Akt regulate chaperone-mediated autophagy. Mol Cell 2015;59:270–84. https://doi.org/10.1016/j.molcel.2015.05.030.
[42] Pedrozo Z, Torrealba N, Fernández C, Gatica D, Toro B, Quiroga C, et al. Cardiomyocyte ryanodine receptor degradation by chaperone-mediated autophagy. Cardiovasc Res 2013;98:277–85. https://doi.org/10.1093/cvr/cvt029.

[43] Ghosh R, Gillaspie JJ, Campbell KS, Symons JD, Boudina S, Pattison JS. Chaperone-mediated autophagy protects cardiomyocytes against hypoxic-cell death. Am J Physiol Cell Physiol 2022;323:C1555–c1575. https://doi.org/10.1152/ajpcell.00369.2021.
[44] Qian L, Zhu Y, Deng C, Liang Z, Chen J, Chen Y, et al. Peroxisome proliferator-activated receptor gamma coactivator-1 (PGC-1) family in physiological and pathophysiological process and diseases. Signal Transduct Target Ther 2024;9:50. https://doi.org/10.1038/s41392-024-01756-w.
[45] Li X, Monks B, Ge Q, Birnbaum MJ. Akt/PKB regulates hepatic metabolism by directly inhibiting PGC-1alpha transcription coactivator. Nature 2007;447:1012–6. https://doi.org/10.1038/nature05861.
[46] Xiong S, Salazar G, San Martin A, Ahmad M, Patrushev N, Hilenski L, et al. PGC-1 alpha serine 570 phosphorylation and GCN5-mediated acetylation by angiotensin II drive catalase down-regulation and vascular hypertrophy. J Biol Chem 2010;285:2474–87. https://doi.org/10.1074/jbc.M109.065235.
[47] Gallardo-Montejano VI, Saxena G, Kusminski CM, Yang C, McAfee JL, Hahner L, et al. Nuclear Perilipin 5 integrates lipid droplet lipolysis with PGC-1α/SIRT1-dependent transcriptional regulation of mitochondrial function. Nat Commun 2016;7:12723. https://doi.org/10.1038/ncomms12723.
[48] Najt CP, Khan SA, Heden TD, Witthuhn BA, Perez M, Heier JL, et al. Lipid droplet-derived monounsaturated fatty acids traffic via PLIN5 to allosterically activate SIRT1. Mol Cell 2020;77:810–824.e8. https://doi.org/10.1016/j.molcel.2019.12.003.
[49] Miner GE, So CM, Edwards W, Ragusa JV, Wine JT, Wong Gutierrez D, et al. PLIN5 interacts with FATP4 at membrane contact sites to promote lipid droplet-to-mitochondria fatty acid transport. Dev Cell 2023;58:1250–1265.e6. https://doi.org/10.1016/j.devcel.2023.05.006.
[50] Kien B, Kolleritsch S, Kunowska N, Heier C, Chalhoub G, Tilp A, et al. Lipid droplet-mitochondria coupling via perilipin 5 augments respiratory capacity but is dispensable for FA oxidation. J Lipid Res 2022;63:100172. https://doi.org/10.1016/j.jlr.2022.100172.
[51] Neubauer S. The failing heart–an engine out of fuel. N Engl J Med 2007;356:1140–51. https://doi.org/10.1056/NEJMra063052.
[52] Ten Hove M, Neubauer S. MR spectroscopy in heart failure–clinical and experimental findings. Heart Fail Rev 2007;12:48–57. https://doi.org/10.1007/s10741-007-9003-8.
[53] D'Souza K, Nzirorera C, Kienesberger PC. Lipid metabolism and signaling in cardiac lipotoxicity. Biochim Biophys Acta 2016;1861:1513–24. https://doi.org/10.1016/j.bbalip.2016.02.016.
[54] Liepinsh E, Makrecka-Kuka M, Volska K, Kuka J, Makarova E, Antone U, et al. Long-chain acylcarnitines determine ischaemia/reperfusion-induced damage in heart mitochondria. Biochem J 2016;473:1191–202. https://doi.org/10.1042/bcj20160164.
[55] Shu S, Cui H, Liu Z, Zhang H, Yang Y, Chen X, et al. Suppression of RCAN1 alleviated lipid accumulation and mitochondrial fission in diabetic cardiomyopathy. Metabolism 2024;158:155977. https://doi.org/10.1016/j.metabol.2024.155977.
[56] Drosatos K, Bharadwaj KG, Lymperopoulos A, Ikeda S, Khan R, Hu Y, et al. Cardiomyocyte lipids impair β-adrenergic receptor function via PKC activation. Am J Physiol Endocrinol Metab 2011;300:E489–99. https://doi.org/10.1152/ajpendo.00569.2010.
[57] Singh RM, Cummings E, Pantos C, Singh J. Protein kinase C and cardiac dysfunction: a review. Heart Fail Rev 2017;22:843–59. https://doi.org/10.1007/s10741-017-9634-3.
[58] Diaz-Vegas A, Madsen S, Cooke KC, Carroll L, Khor JXY, Turner N, et al. Mitochondrial electron transport chain, ceramide and coenzyme Q are linked in a pathway that drives insulin resistance in skeletal muscle. bioRxiv 2023. https://doi.org/10.1101/2023.03.10.532020.